Estimating the location of a causative body from a self-potential anomaly using 2D and 3D normalized full gradient and Euler deconvolution

Petek SINDIRGI* , Şenol ÖZYALIN

Department of Geophysical Engineering, Faculty of Engineering, Dokuz Eylül University, İzmir, Turkey

Abstract: Changes in the size and depth of sources greatly affect self-potential (SP) anomalies. Therefore, it is important to determine the location of the source accurately. In the present study, applications of the normalized full gradient (NFG) method and Euler deconvolution (EUD) were described to determine the location of the sphere-like SP body as complementary approaches to other optimization algorithms. The NFG and EUD methods were tested on synthetic, noise-free, and noisy anomalies caused by sphere-like models in two-dimensional (2D) and three-dimensional (3D) cases. Subsequently, the methods were applied to real field data. The importance of the present study lies in the fact that it is the first 3D application of these methods to the SP anomaly caused by the sphere-like model in the literature. In order to determine the optimum harmonic number in the NFG method, a new criterion was used instead of the usual trial-and-error method, providing more reliable selection possibilities. In a similar way, average values were used to determine the window size accurately in the EUD method. The test results of the synthetic and real field models were satisfactory. They showed that both methods are applicable to determine the location of sphere-like structures, such as ore deposits, in self-potential surveys.

Key words: Self-potential, normalized full gradient, Euler deconvolution, optimum harmonic number, optimum window size

1. Introduction

The self-potential (SP) method has a variety of application in geophysics including mining (Yüngül, 1950; Paul, 1965; Essa et al., 2008; Mendonça, 2008; Fedi and Abbas, 2013; Essa and Elhussein, 2017), groundwater (Bogoslovsky and Ogivly, 1973; Revil and Jardani, 2013), and geothermal surveys (Sill, 1983; Corwin, 1990; Schima et al, 1996; Yasukawa et al., 2003). A number of researchers have calculated potential distributions over polarized bodies having simple geometries, such as spheres, cylinders, and dipoles, by simplifying the potential of the sources and making assumptions about them (Yüngül, 1950; Mohan and Singh, 1972; Bhattacharya and Roy, 1981; Rao and Babu, 1983; Roy and Mohan, 1984; Abdelrahman and Sharafeldin, 1997).

Several methods have been introduced for the interpretation of SP data; some of them use graphics-based techniques, such as the characteristic point method (Paul, 1965; Paul et al., 1965; Rao et al., 1970), logarithmic-curve matching (Meiser, 1962; Murthy and Haricharan, 1984), and nomograms (Bhattacharya and Roy, 1981; Murthy and Haricharan, 1985). Recent methods include least-squares inversion (El-Araby, 2004; Essa et al., 2008),

the Fourier and Hilbert transforms (Sundararajan et al., 1990; Sundararajan and Narasimha Chary, 1993; Asfahani et al., 2001; Di Maio et al., 2016; Di Maio et al., 2017b), gradient and derivative analysis (Abdelrahman et al., 1997, 1998, 2003), the normalized full gradient (NFG) method (Sındırgı et al., 2008; Abedi et al., 2012), enhanced local wavenumber technique (Srivastava and Agarwal, 2009), extended Euler deconvolution (EUD) (Agarwal and Srivastava, 2009), and global optimization algorithms such as particle swarm optimization (PSO), genetic algorithm (GA), differential evolution (DE), and adaptive simulated annealing (Abdelazeem and Gobashy, 2006; Tlas and Asfahani, 2008; Fernández-Martínez et al., 2010; Santos, 2010; Pekşen et al., 2011; Göktürkler and Balkaya, 2012; Balkaya, 2013; Biswas and Sharma, 2015; Di Maio et al., 2017a).

The NFG method has been adopted since the 1960s and is particularly applicable when determining the singular points of potential fields (Golizdra, 1962; Strakhov, 1962; Berezkin, 1967; Strakhov et al., 1977; Mudretsova et al., 1979; Ciancara and Marcak, 1979; Berezkin, 1988; Pašteka, 1996; Pašteka, 2000; Zeng et al., 2002; Özyalın, 2003; Sındırgı et al., 2008). It integrates the analytical signal and

---

the downward continuation. This method has been widely used to interpret 2D potential field data (Hou and Shi, 1986; Ebrahimzadeh Ardestani, 2004; Dondurur, 2005; Aydın, 2007, 2010; Oruç and Keskinsezer, 2008; Sındırgı et al., 2008; Aghajani et al., 2009, 2011; Fedi and Florio, 2011; Zhou, 2015).

The EUD method is based on the Euler homogeneity relation (Thompson, 1982) and is employed to estimate the accurate origin and depth of the potential field source. Since the 1990s, 2D and 3D implementations of EUD on gravity and magnetic potential sources have been widely used (Reid et al., 1990; Paterson et al., 1991; Roest et al., 1992; Beasley and Golden, 1993; Hearst and Morris, 1993; Fairhead et al., 1997; Zhang et al., 2000; Mushayandebvu et al., 2001; Silva et al., 2001; Silva and Barbosa, 2003; Fitzgerald et al., 2004; Keating and Pilkington, 2004; Al-Saud, 2014; Ekinci et al., 2017). This method uses potential field data and their first-order derivatives in a system of linear equations. It is closely related to Euler's homogeneity equation and the structural index (SI); the SI is associated with the source geometry (Gerovska and Arauzo-Bravo, 2003; Dewangan et al., 2007; Ekinci et al., 2014; Rabeh and Khalil, 2015).

In the present study, 2D and 3D NFG and EUD methods were applied to synthetic and field anomalies in order to present a new and robust approach for the detection of SP source location. The methods were tested on a field dataset from Turkey known as the Süleymanköy anomaly, Ergani (Yüngül, 1950). The results are discussed herein. The present study is the first 3D application of the proposed methods to the SP anomaly caused by the sphere-like model in the literature, and it shows that they can be used as complementary approaches to the other solution techniques for estimating the SP source location in 2D and 3D cases.

2. Materials and methods

2.1. Definition of the SP anomaly
The SP anomaly at any point on the earth's surface, caused by a simple geometrical polarized body, can be presented as follows (Yüngül, 1950; Murthy and Haricharan, 1985) (Figure 1):

$$V(x, x_0, K, z_0, q) = K \frac{(x - x_0)\cos\theta + z_0\sin\theta}{\left[(x - x_0)^2 + z_0^2\right]^q} \quad (1)$$

where x is the horizontal distance, x_o is the exact origin of the anomaly, K is the electric dipole moment, θ is the polarization angle, z_0 is the depth of the center of the body, and q is the dimensionless shape factor. The parameter q is 0.5 for a semiinfinite vertical cylinder, 1.0 for an infinitely long horizontal cylinder, and 1.5 for a sphere. Examples of noise-free and noisy anomalies belonging to
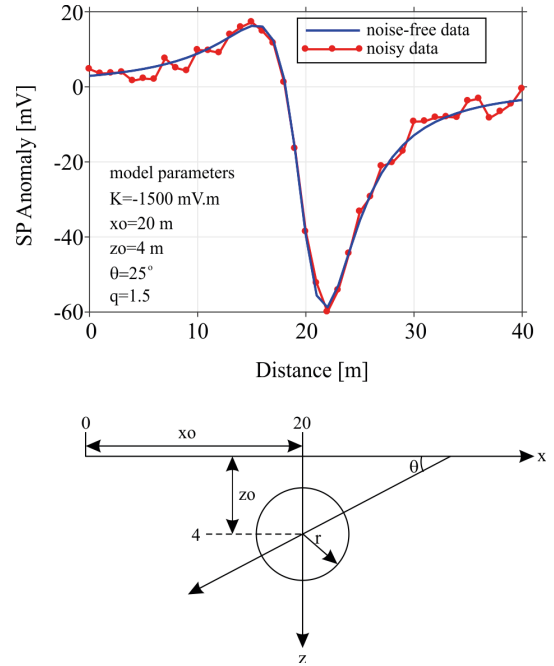

Figure 1. Schematic illustration of the geometry of a 3D single buried sphere model (lower panel) and 2D noise-free and noisy SP anomalies used in the tests with the synthetic data (upper panel).

a sphere model are illustrated in Figure 1, upper panel. In the present study, a value of 1.5 was assigned to q for the sphere model and thus, for the 2D and 3D sphere models, Eq. (1) transforms into

$$V(x, x_0, K, z_0) = K \frac{(x - x_0)\cos\theta + z_0\sin\theta}{\left[(x - x_0)^2 + z_0^2\right]^{1.5}} \quad (2)$$

$$V(x, x_0, K, y, y_0, z_0) = K \frac{(x - x_0)\cos\theta + z_0\sin\theta}{\left[(x - x_0)^2 + (y - y_0)^2 + z_0^2\right]^{1.5}} \quad (3)$$

Noise-free theoretical data to be used in the application of the NFG and EUD methods were generated from the equations above. For noisy data, the noise (which comprised normally distributed, zero-mean pseudorandom numbers with a standard deviation of ±5 mV) was also added to the SP anomaly.

2.2. The NFG method
Fundamentally, the NFG method is based on the downward continuation of the potential field data and its analytic signal amplitude (ASA). In many studies, it has been proved that this method is highly applicable in determining the source location and depth, by using potential field anomalies (Zeng et al., 2002; Özyalın, 2003;

Aydın, 2007; Oruç and Keskinsezer, 2008; Sındırgı et al., 2008; Ekinci and Yiğitbaş, 2012, 2015; Zhang and Meng, 2015; Ekinci et al., 2017) and they include the detailed formulation of the method. That is why the 3D situation will be emphasized in this section.

The 2D NFG operator is defined as follows (Berezkin, 1967, 1973):

$$
NFG(x,z) = \frac{\sqrt{\left[\left(\frac{\partial V(x,z)}{\partial x}\right)^2 + \left(\frac{\partial V(x,z)}{\partial z}\right)^2\right]^v}}{\frac{1}{M}\sum_{i=1}^{M}\sqrt{\left[\left(\frac{\partial V(x,z)}{\partial x}\right)^2 + \left(\frac{\partial V(x,z)}{\partial z}\right)^2\right]^v}}
$$

(4)

whereis NFG (x,z) the NFG amplitude at point (x,z) and $V(x,z)/\partial x$ and $V(x,z)/\partial z$ are the horizontal and vertical derivatives of the potential field anomalies, respectively. M represents the number of observation points, z is the downward continuation level, and u is the degree of the NFG operator controlling the peak amplitude value and peak anomaly width of the NFG sections (Dondurur, 2005; Sındırgı et al., 2008). The denominator of Eq. (4) is the mean value of the ASA and this normalization makes the NFG amplitude dimensionless. When the NFG contour values are greater than 1, they are taken to be the maxima and those smaller than 1 represent the minima (Dondurur, 2005).

Similarly, the 3D form of the 2D definition of the NFG operator at a specific point (x, y, z) is given as follows (Zeng et al., 2002; Tran, 2004):

$$
NFG(x,y,z) = \frac{\sqrt{\left[\left(\frac{\partial V(x,y,z)}{\partial x}\right)^2 + \left(\frac{\partial V(x,y,z)}{\partial y}\right)^2 + \left(\frac{\partial V(x,y,z)}{\partial z}\right)^2\right]^v}}{\frac{1}{M}\sum_{i=0}^{M}\sqrt{\left[\left(\frac{\partial V(x,y,z)}{\partial x}\right)^2 + \left(\frac{\partial V(x,y,z)}{\partial y}\right)^2 + \left(\frac{\partial V(x,y,z)}{\partial z}\right)^2\right]^v}}
$$

(5)

The downward continuation process can be obtained by the Fourier series summation, and for the 3D case the potential function $V(x, y, z)$ for any harmonic limit ranges in the x- (N_1, N_2) and y-direction (M_1, M_2) is defined as follows (Berezkin, 1988):

$$
V(x,y,z) = \sum_{n=N_1}^{N_2}\sum_{m=M_1}^{M_2} B_{nm}\sin\left(\frac{\pi n}{L_1}x\right)\sin\left(\frac{\pi m}{L_2}y\right)e^{\frac{\pi(n+m)z}{L_1 L_2}} k
$$

(6)

In this equation, B_{nm} is the Fourier sine coefficient, n and m are the harmonic numbers, and L_1 and L_2 are the Fourier sine series ranges along the x- and y-directions, respectively. z is the downward continuation level and k is the Lanczos smoothing term, which eliminates the Gibbs effect (Berezkin, 1988) and is defined as

$$
k = \left[\frac{\sin(\frac{\pi(n+m)}{NM})}{\frac{\pi(n+m)}{NM}}\right]^\mu
$$

(7)

where m is defined as the degree of smoothing and is generally assigned a value of 1 or 2. In the present study, a value of 2 was chosen. B_{nm} is also formulated as

$$
B_{nm} = \frac{4}{L_1 L_2}\sum_{0}^{L_1}\sum_{0}^{L_2} V(x,y,0)\sin\left(\frac{\pi n}{L_1}x + \frac{\pi m}{L_2}y\right)
$$

(8)

The harmonic limits are usually determined by the trial-and-error method. In general, a value of 1 is assigned to N_1 and a value of N_2 is then determined by giving some values in ascending order (Özyalın, 2003; Dondurur, 2005; Aydın, 2007; Sındırgı et al., 2008). Some closed contours are produced around the body for all harmonic limits. Principally, the center of the completely closed, symmetric contours indicates the local maximum and two adjacent minima enclosures define the actual location parameters of the body (Özyalın, 2003; Aydın, 2007; Sındırgı et al., 2008). In the present study, the limit values of the harmonics in both the synthetic and field data were determined using this procedure.

The derivatives of $V(x, y, z)$ along the x, y, and z directions, respectively, can be written as

$$
\frac{\partial V(x,y,z)}{\partial x} = \frac{\pi}{L_1}\sum_{n=N_1}^{N_2}\sum_{m=M_1}^{M_2} nB_{nm}\cos\left(\frac{\pi n}{L_1}x\right)\sin\left(\frac{\pi m}{L_2}y\right)e^{\frac{\pi(n+m)z}{L_1 L_2}} k
$$

(9)

$$
\frac{\partial V(x,y,z)}{\partial y} = \frac{\pi}{L_2}\sum_{n=N_1}^{N_2}\sum_{m=M_1}^{M_2} mB_{nm}\sin\left(\frac{\pi n}{L_1}x\right)\cos\left(\frac{\pi m}{L_2}y\right)e^{\frac{\pi(n+m)z}{L_1 L_2}} k
$$

(10)

$$
\frac{\partial V(x,y,z)}{\partial z} = \frac{\pi(n+m)}{L_1 L_2}\sum_{n=N_1}^{N_2}\sum_{m=M_1}^{M_2} B_{nm}\sin\left(\frac{\pi n}{L_1}x\right)\sin\left(\frac{\pi m}{L_2}y\right)e^{\frac{\pi(n+m)z}{L_1 L_2}} k
$$

(11)

Substituting Eqs. (9), (10), and (11) into Eq. (5), the NFG can be calculated.

The harmonic number is important in the calculation of the Fourier series. In the literature, the number of harmonics (N) is generally determined by the trial-and-error method. In this method, to determine the optimum harmonic number the map, which identifies the most compact body from closed contours for many harmonics, is specified. The trials and the resulting maps from them are obtained for each harmonic in sequence. Different from the previous studies by Özyalın (2003), Aydın (2007), Sındırgı et al. (2008), etc., in the present study, the optimum value of the harmonic number in the Fourier series (N) (in 2D) was determined with a criterion based on the calculation of the minimum error variation without need for repeated

trials. The CPU time was only 13.4 s for NFG calculation of the synthetic model in 2D, for N = 5–28. The minimum error was obtained by dividing the standard deviation of the depth values corresponding to 1 maximum and 2 minima in the NFG sections by the maximum amplitude of the depth value. By calculating the minimum error values corresponding to different harmonic numbers, the lowest error expresses the optimum number of harmonics.

If we used the trial-and-error method for our 2D synthetic model data we would spend 24 harmonics ´ 10 s = 240 s CPU time (N = 5–28) for only calculation; then we would also decide on the optimum N value by visual examination of NFG sections. This process would also take some time.

We did not use the minimum error calculation for determining the optimum harmonic number in the 3D case, because the 3D NFG applications are required to be done separately for each depth section, and in this case it spends more CPU time (for example, required CPU time for our 3D synthetic model: 24 harmonics ´ 13.4 s = 322 s plus visual examination of NFG sections one by one using an Intel Core i5 computer with 8 GB RAM). Instead, we chose and applied the method based on the maximum amplitude developed by Aghajani et al. (2009). The CPU time for that method was calculated as 293 s. This method is applied to a SP anomaly for the first time in our study.

In order to detect the optimum harmonic number, this method uses changes in the NFG amplitude and the harmonic number. The maximum NFG amplitude value, using harmonic numbers, is computed and the variations in the NFG versus harmonic number are then plotted. It is considered the greatest amplitude occurs versus the optimum harmonic number (Aghajani et al., 2009).

2.3. EUD method
The horizontal location and depth of the potential field source can be estimated by the EUD method. The proposed method uses Euler's homogeneity equation (Thompson, 1982) on a moving data window with a given structural index (SI) (Gerovska and Arauzo-Bravo, 2003; Dewangan et al., 2007; Agarwal and Srivastava, 2009; Ekinci et al., 2014). If $V(x, y, z)$ is the self-potential observed at a (x, y, z) measuring point, due to the electric charge distribution at point (x_0, y_0, z_0), then the 2D (Thompson, 1982) and 3D (Reid et al., 1990) Euler homogeneity equations can be written as

$$x_0 \frac{\partial V}{\partial x} + z_0 \frac{\partial V}{\partial z} = x \frac{\partial V}{\partial x} + NV \qquad (12)$$

and

$$(x - x_0) \frac{\partial V}{\partial x} + (y - y_0) \frac{\partial V}{\partial y} + (z - z_0) \frac{\partial V}{\partial z} = -NV \quad (13)$$

where N is a structural index that defines the anomaly attenuation rate at the observation point; the unknown

parameters x_0, y_0, and z_0 can be calculated from the solution of the linear systems of equations generated from Eq. (13). In the present study, a value of 1.5 was assigned to N for a SP anomaly due to a sphere-like model.

In the EUD, it is important to determine the optimum window size and generally the trial-and-error method is used for this. In the present study, the optimum window size was obtained from a different point of view. A technique was developed to determine the optimum window size by calculating the average of the depths (or distances) for each selected window size. The variations in the calculated average of the depths (or distances) versus window size were plotted. The mean value of the depths (or distances) was also plotted as a line. Accordingly, the window size that intersects the mean value line was regarded as being the optimum. In cases with too many cutting points, the window size with the common cut point was selected for the whole parameter (z_0, x_0, and y_0).

3. Synthetic examples
In this section, the applicability of the NFG and the EUD methods in 2D (and particularly in 3D) for a simple sphere model was investigated. In order to test the effect of the proposed methods in determining the location parameters, such as the depth of the body center and the distances from the origin, a synthetic sphere model was calculated. After adding noise to synthetic anomalies, the proposed methods were tested by estimating the model location parameters of the SP source body.

3.1. NFG method applications to 2D synthetic data
First, the success of the NFG and the EUD methods was tested by detecting the location parameters of a noise-free SP anomaly, produced by a spherical body (Figure 1, lower panel) sampled at 41 points over a 40-m profile and at 1-m intervals. The parameters used for this model were selected as follows: $K = -1500$ mV m, $z_0 = 4$ m, $x_0 = 20$ m, $\theta = 25°$, and $q = 1.5$ (Figure 1, upper panel).

Thereafter, to calculate the noisy synthetic model, the normally distributed, zero-mean pseudorandom numbers, with a standard deviation of ±5 mV, were added to the synthetic data (Figure 1, upper panel).

The NFG models were created for the noise-free synthetic model by using different harmonic numbers (for harmonics from 5 to 28). Based on the criteria that were developed, minimum error values were calculated, corresponding to each harmonic number (Figure 2a). It can be seen that the observed minimum error value is at the 19th harmonic. Similar to the noise-free model, and also for noisy data, the NFG method was applied to the same harmonic range. Minimum error values corresponding to each harmonic number were also calculated for noisy synthetic data (Figure 2b). The minimum error value is smallest at the 16th harmonic.

In Figure 3a, the NFG cross sections that were calculated for the noise-free, synthetic model are given for the harmonic numbers 15, 19, 23, and 27. The minimum and maximum NFG singular values in the sections are marked as white dots. The depth (z_0) and distance (x_0) values obtained from the

NFG solution for the 19th harmonic value of the synthetic data are 4.0 m and 20.0 m, respectively (Table 1). These values are the same as the initial model parameters.

In Figure 3b, the NFG cross sections are given for the 12, 16, 20, and 24 harmonic numbers selected
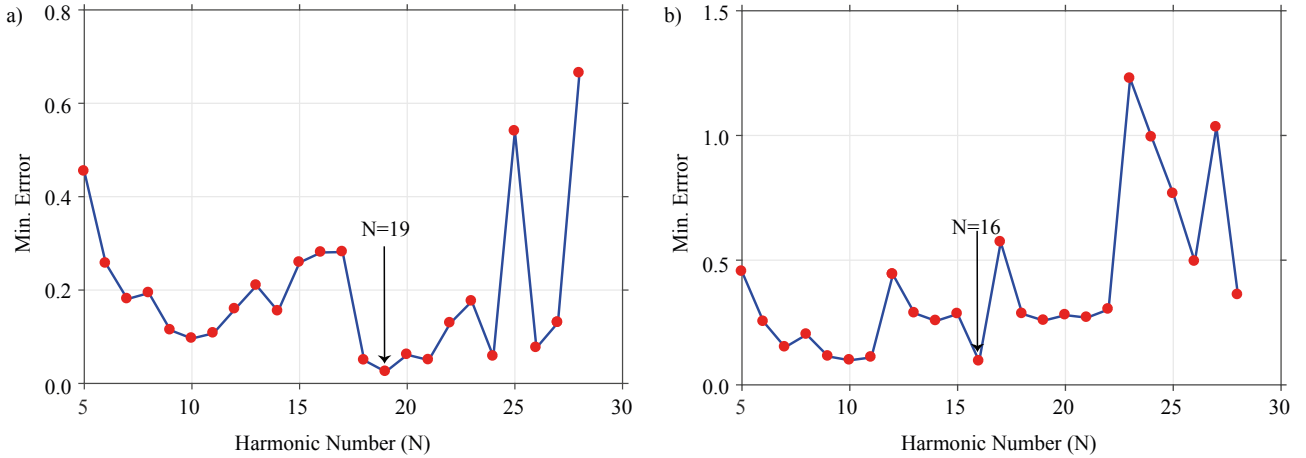
Figure 2. The variation in minimum error values versus harmonic numbers (N) for a) noise-free and b) noisy synthetic data.
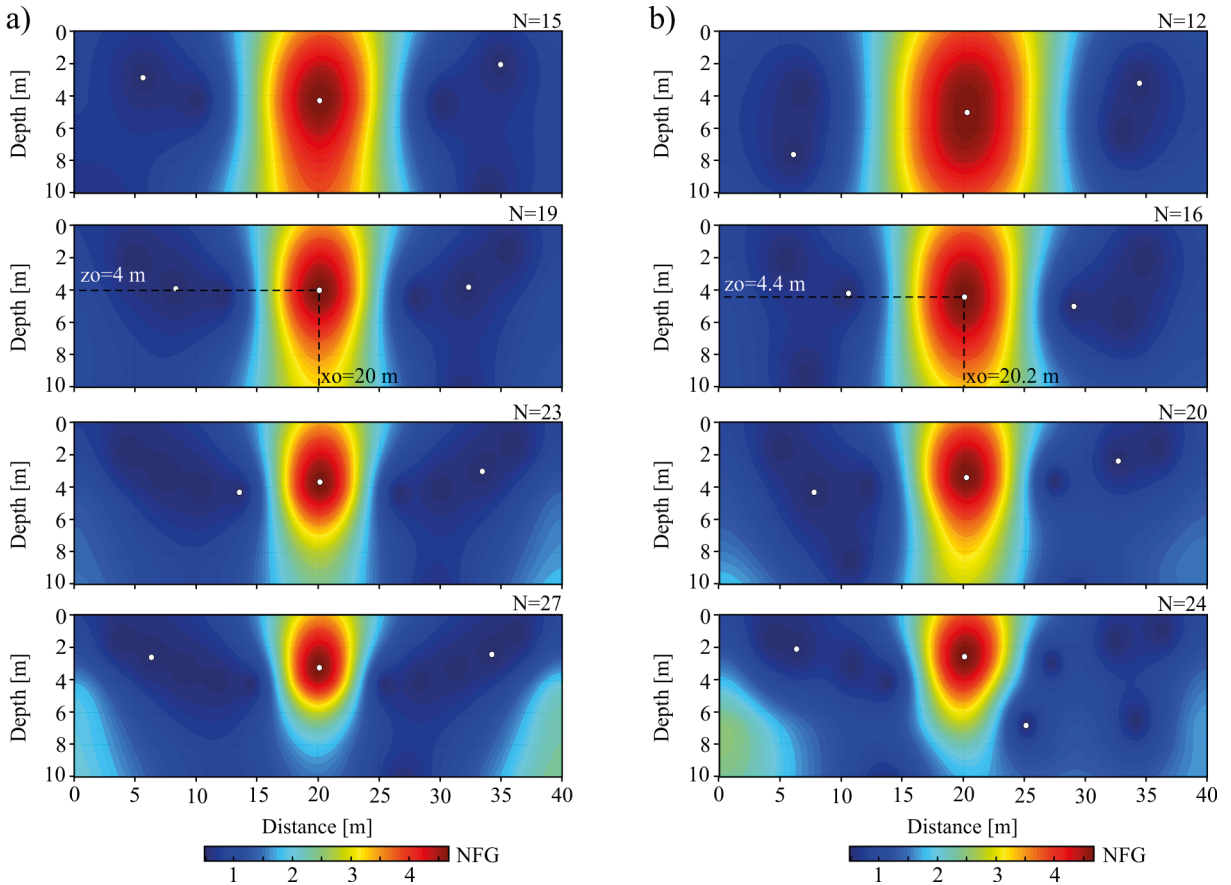

Figure 3. NFG sections for a single 2D synthetic sphere model for various harmonics: a) in the case of noise-free data, the optimum value of N was found to be 19; b) in the case of noisy data, the optimum value of N was found to be 16.

Table 1. The best model parameters obtained from the NFG and EUD algorithms for the synthetic noise-free and noisy datasets (2D).

Case	Model par.	Synthetic anomaly	NFG	EUD
Noise-free	z_0 [m]	4.0	4.0	4.01
	x_0 [m]	20.0	20.0	20.15
Noisy	z_0 [m]	4.0	4.4	3.94
	x_0 [m]	20.0	20.2	20.24

from these harmonics. The depth (z_0) and distance (x_0) values obtained from the NFG solution for the 16th harmonic of the synthetic data are 4.4 m and 20.2 m, respectively (Table 1). Since the data contain noise, the calculated values differ from the initial model parameters by 9% of the depth value and 1% of the distance value.

3.2. EUD method applications to 2D synthetic data
Firstly, the EUD method was applied to the same noise-free, synthetic data used in the NFG application. The window size was selected between 6 and 40 (Figure 4). In order to determine the optimum window size, the recommended approach was used instead of the trial-and-error method. In Figure 4, the average value is indicated by the green line and the depth or horizontal distance values were calculated for each window size, as indicated by red dots.

From the window sizes between 6 and 40 (which are shown in Figure 4a), the calculated horizontal distance for window size 6 is 19.6 m, while for window size 40 the horizontal distance was calculated as 20.2 m. In order to avoid this discrepancy, the average values were also calculated. Using the suggested method instead of the trial-and-error technique, the horizontal distance (x_0) from the origin was calculated as 20.15 m (0.7%) with 0.7% error (Figure 4a) and the depth (z_0) was 4.01 m with 0.2% error (Figure 4b). The average window size for the noise-free model was determined as 17. The common solution of the horizontal distance from the origin and the depth from the surface are shown in Figure 4c.

The EUD method was also applied to the same noisy, synthetic data used in the NFG application. The horizontal distance (x_0) from the origin was calculated as 20.24 m (0.7%) with 1.1% error (Figure 4d) and the depth (z_0) was 3.94 m with 1.5% error (Figure 4e). It is clear from Figures 4d and 4e that the common window size is 16. The common solution for horizontal distance and depth is shown in Figure 4f. The calculated model parameters for the 2D case with the NFG and the EUD methods are shown in Table 1.

3.3. NFG method applications to 3D synthetic data
In this section, the 3D noise-free, synthetic SP sphere anomaly, sampled at 41×41 points with a 1-m interval, was calculated first. Secondly, the NFG and the EUD methods were applied to test their success. The parameters used for this model were as follows: $K = -1500$ mV m, $\theta = 25°$, $z_0 = 4$ m, $q = 1.5$, $x_0 = 20$ m, and $y_0 = 20$ m. Finally, the noise (which occurred as normally distributed, zero-mean pseudorandom numbers with a standard deviation of ± 5 mV) was also added to the synthetic SP anomaly. Noise-free and noisy anomalies are shown in Figures 5a and 5b, respectively.

In the NFG method solutions, the harmonic numbers were chosen between 2 and 25, according to the maximum amplitude method (Aghajani et al., 2009). The variations in the NFG amplitudes versus harmonic numbers ($N = 2$ to 25) for noise-free data are plotted in Figure 6a. It can be seen from Figure 6a that the maximum NFG amplitude value ($A = 10.4$) was calculated at the 19th harmonic. The variations in the maximum amplitudes versus depths for noise-free data are plotted in Figure 6b. For each harmonic number, the depth increment was chosen as 0.5 m. Figure 6b shows that the maximum NFG amplitude ($A = 10.4$) calculated for N = 19 is caused by a body that has a center depth of 4.0 m. This value was also matched with the depth parameter of the synthetic data.

Similarly, the variations in the NFG amplitudes versus harmonic numbers ($N = 2$ to 25) for noisy synthetic data is plotted in Figure 6c. The maximum amplitude value ($A = 10.2$) was calculated at the 16th harmonic. The variations in the maximum NFG amplitudes versus depths for noisy data are plotted in Figure 6d. The maximum NFG amplitude ($N = 16$) matches with the $z_0 = 4.5$ m depth. Due to the added noise, the maximum amplitude changed, and the depth was calculated as 4.5 m.

For noise-free synthetic data, when the NFG solutions were plotted at various depths for the 19th harmonic (Figure 7), the full contour closure appeared to be 4.0-m deep. The coordinates of the maximum value ($x_0 = 20$ m, $y_0 = 20$ m) were matched with the model coordinates.

For noisy synthetic data, when the NFG solutions were plotted at various depths for the 16th harmonic (Figure 8), the full contour closure (i.e. the maximal enclosure location) appeared to be 4.5-m deep. The coordinates of this maximal NFG enclosure location were determined as being $x_0 = 19$ m, $y_0 = 21$ m.

3.4. EUD method applications to 3D synthetic data
Using the proposed approach instead of the trial-and-error method, the EUD method was applied to the noise-free synthetic anomaly. The window size was selected between 3 and 40 (Figure 9). In Figure 9, the average value is indicated by the green line and the depth or horizontal distance values calculated for each window size are indicated by red dots.
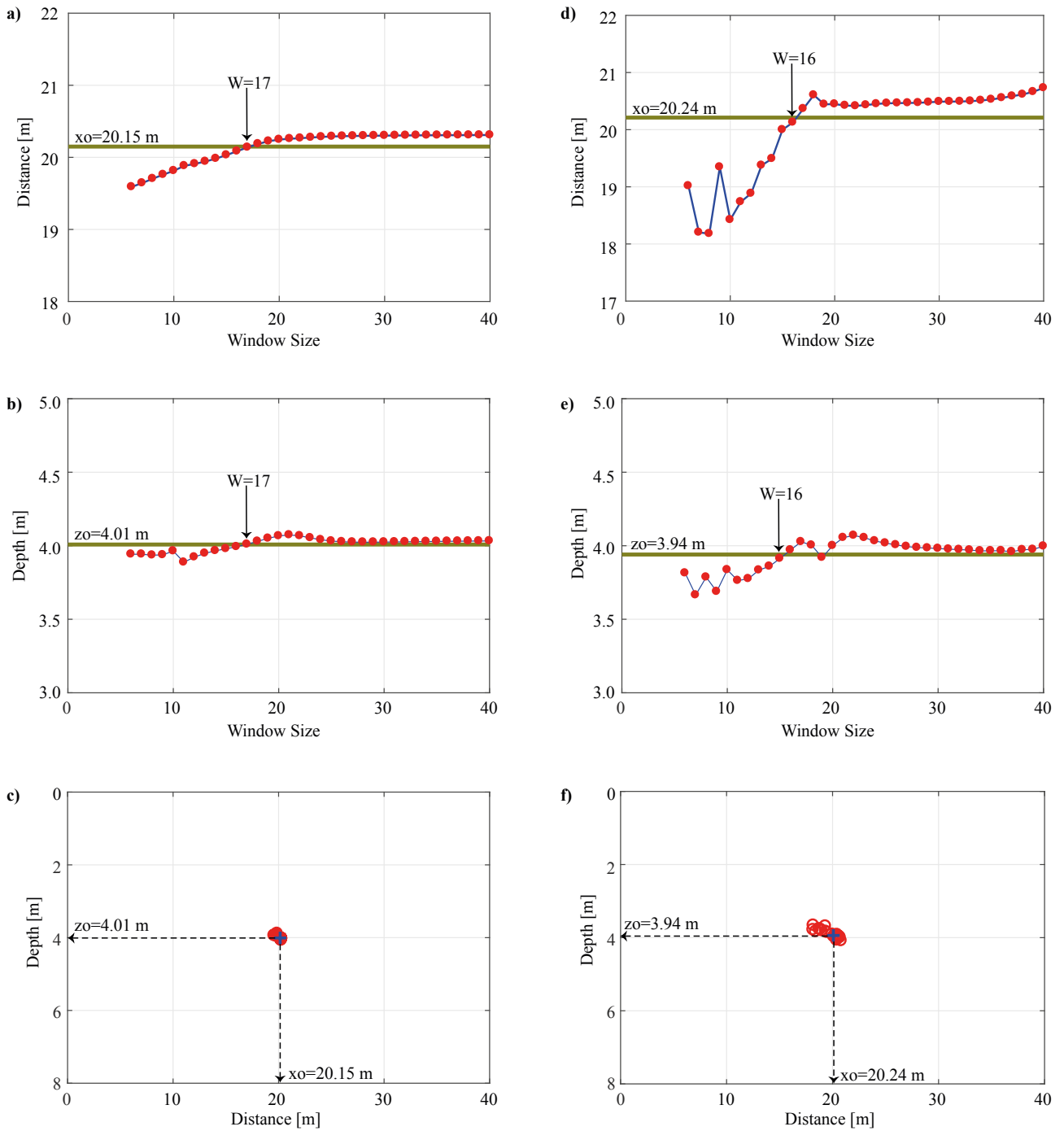
Figure 4. EUD solutions of the synthetic 2D sphere model using average value calculation. In the case of noise-free data, determination of the window size a) according to the horizontal distance (x_0), b) according to the depth (z_0), and c) common solution of depth and horizontal distance. In the case of noisy data, determination of the window size d) according to the horizontal distance (x_0), e) according to the depth (z_0), and f) common solution of depth and horizontal distance.

From window sizes between 3 and 40 (which are shown in Figure 4a), the calculated depth for window size 3 was 20.1 m, while for window size 40 the depth was calculated as 19.9 m. The average values were calculated similarly to

the 2D case. With the developed method being applied (instead of the trial-and-error technique), the horizontal distances from the origin were calculated as x_0 = 20.04 m with 0.20% error (Figure 9a) and y_0 = 20.19 m with 0.95%
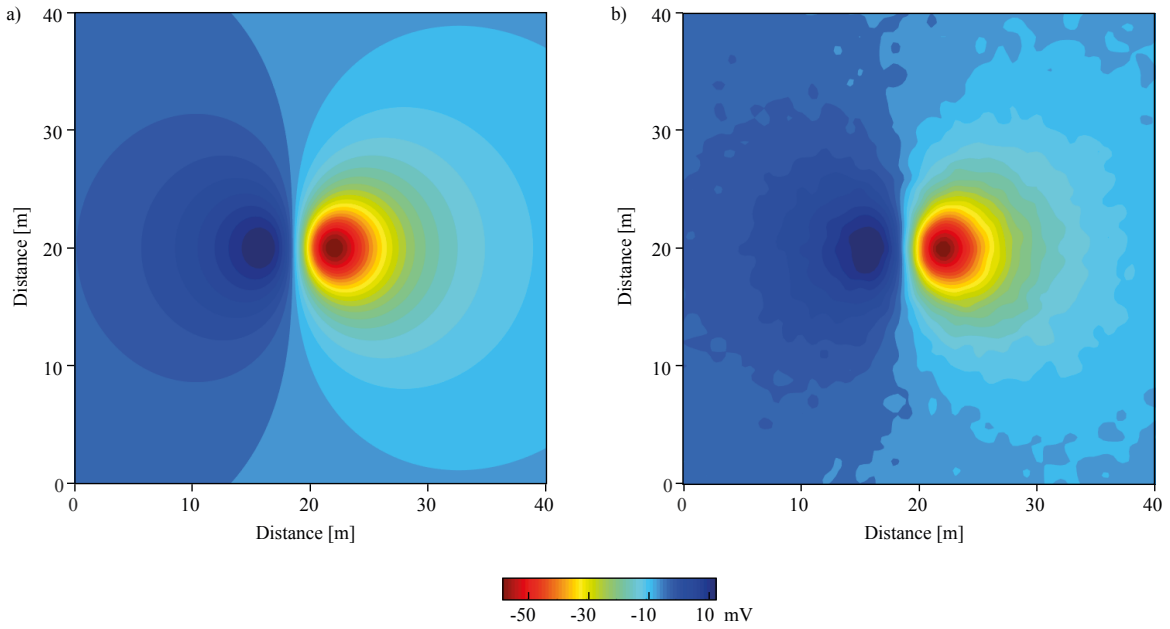
Figure 5. Anomaly maps of 3D synthetic data: a) noise-free and b) noisy.
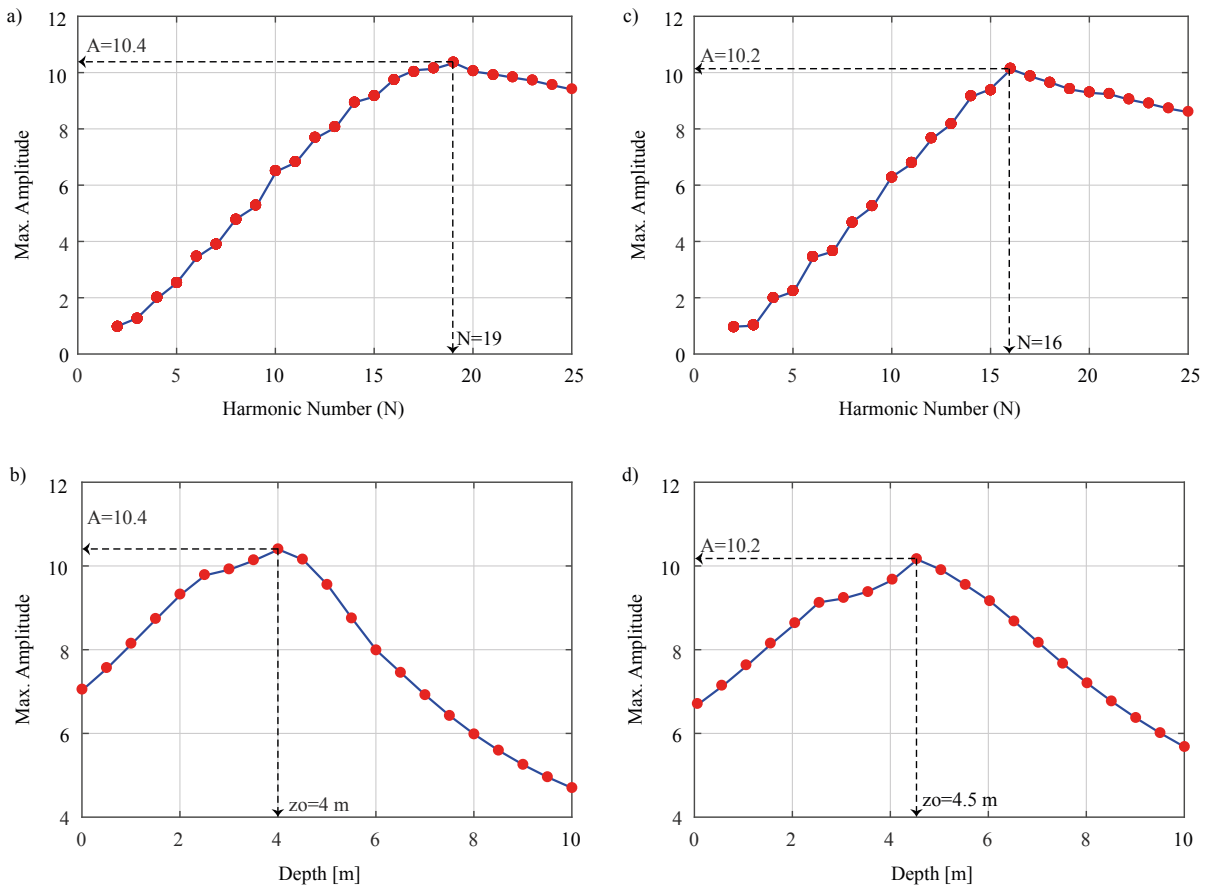

Figure 6. In the case of noise-free data, a) harmonic number ($N = 19$) and maximum amplitude determination procedure and b) the depth corresponding to the maximum amplitude. In the case of noisy data, c) harmonic number ($N = 16$) and maximum amplitude determination procedure and d) the depth corresponding to the maximum amplitude.
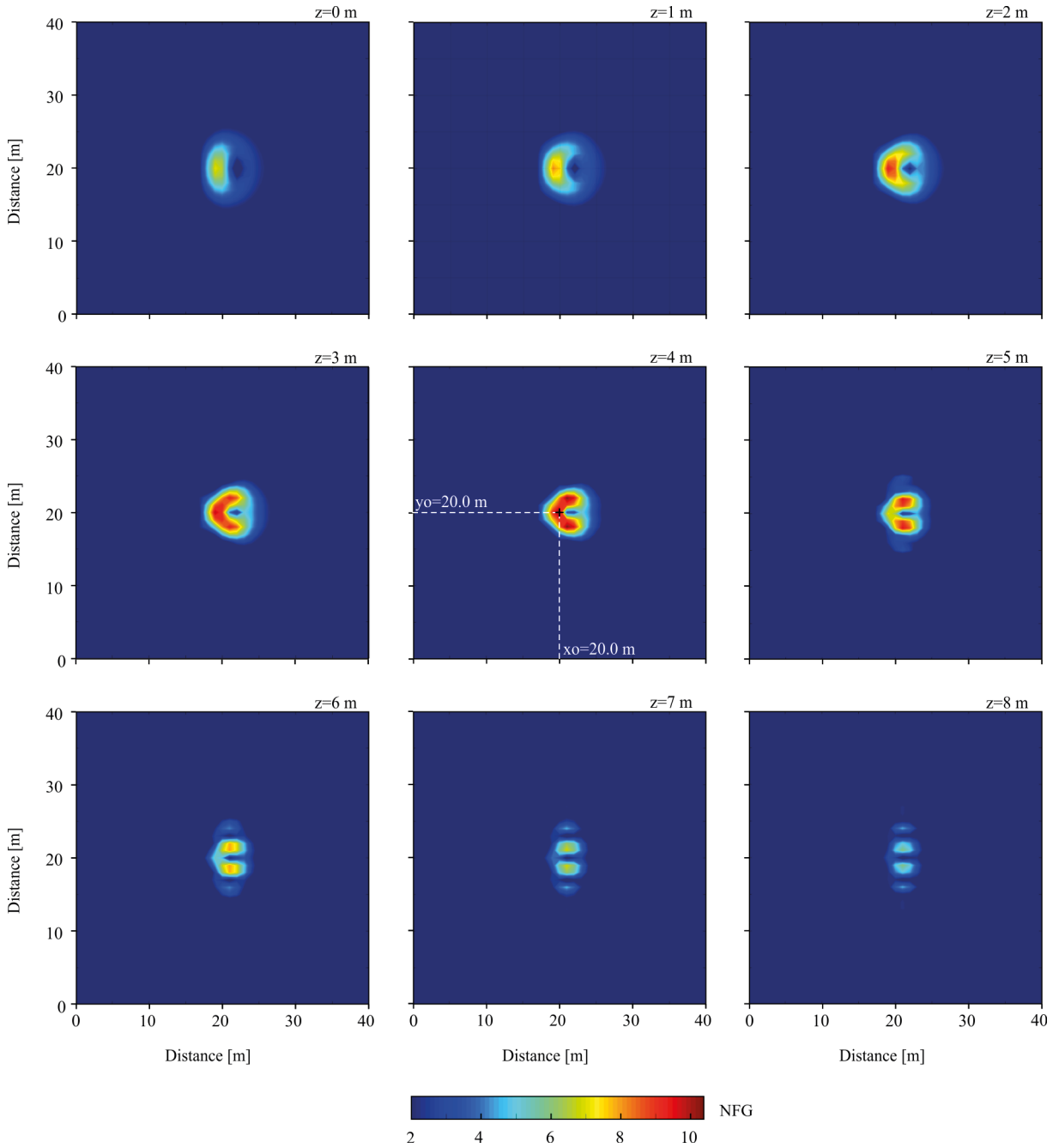
Figure 7. NFG solutions of the noise-free synthetic SP anomaly at various depths for the 19th harmonic.

error (Figure 9b). The depth (z_0) was 4.01 m with 0.20% error (Figure 9c). This corresponded to average window size 20 for the noise-free model. The EUD method was also applied to the noisy 3D theoretical anomaly. The horizontal distances from the origin were calculated as x_0 = 19.85 m (Figure 9d) and y_0 = 20.24 m with 1.20% error (Figure 9e) and the depth (z_0) was 3.85 m with 3.70% error (Figure 9f). It is clear from Figures 9d–9f that the common window size is 20.

The common solutions of the noisy and noise-free data are shown in Figures 10a–10f, respectively. Calculated model parameters for the 3D cases with the NFG and the EUD methods are shown in Table 2.

4. Field studies
The Ergani-Süleymanköy copper field example in Turkey (Yüngül, 1950) is often used in the literature and it was used here to test the efficiency of the NFG and EUD
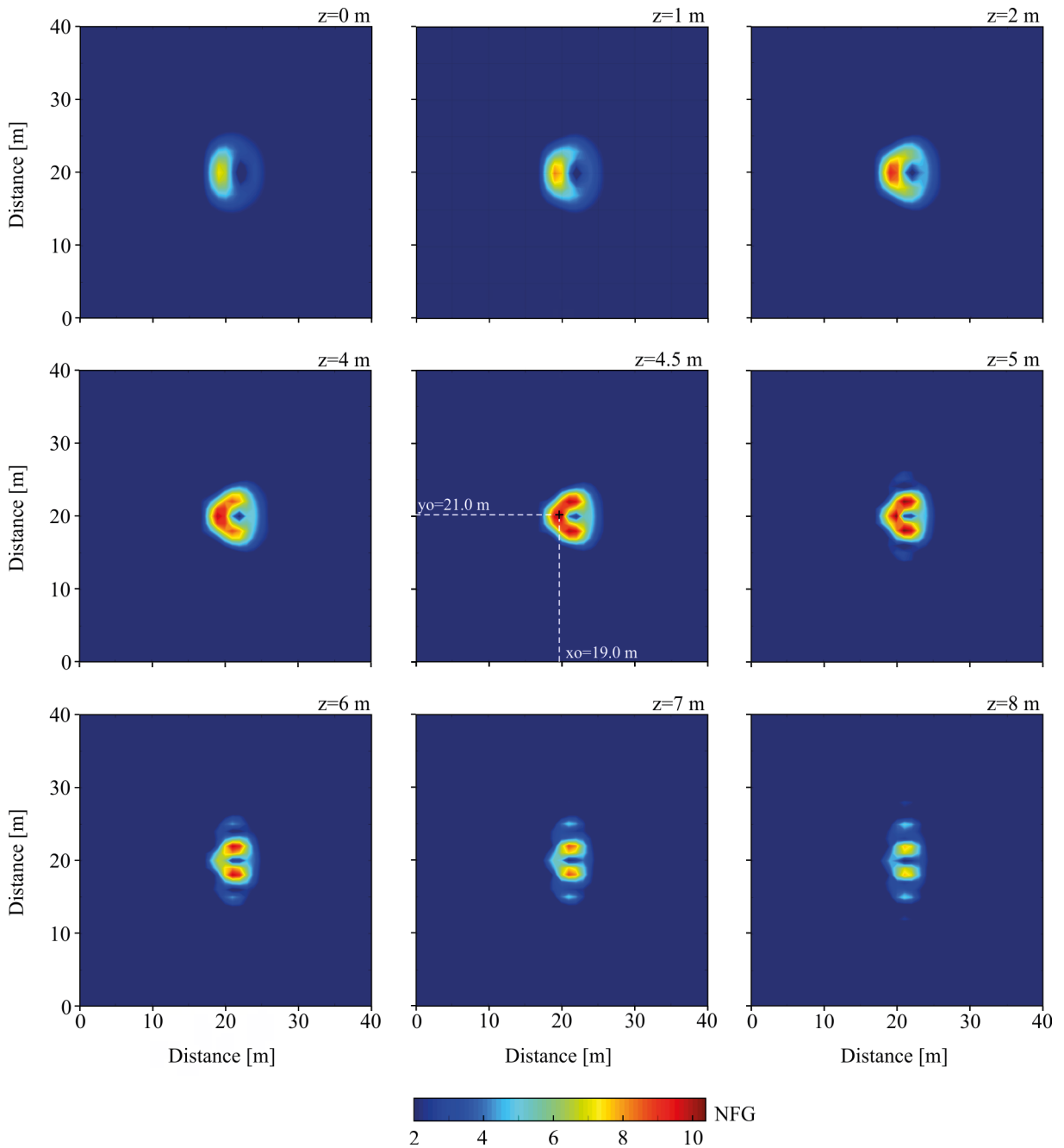
Figure 8. NFG solutions of the noisy synthetic SP anomaly at various depths for the 16th harmonic.

methods. The Süleymanköy copper field metallic sulfide deposits are located 65 km southeast of the city of Elazığ, in eastern Turkey. The observed SP anomaly map and the selected A-B cross-section are shown in Figures 11a and 11b, respectively (Yüngül, 1950). The anomaly was identified by the positive (max. amplitude ~100 mV) and negative (max. amplitude ~−225 mV) SP values along the profile. The anomaly in Figure 11a was digitized at 5-m intervals for 3D interpretation. The A-B cross-section

anomaly (Figure 11b) was digitized at 1-m intervals for 2D interpretation along a profile of 250 m.

The 2D NFG and EUD methods were applied to the A-B cross-section anomaly. Then the 3D NFG and EUD methods were applied to the SP anomaly in Figure 11a.

For the application of the 2D NFG method, harmonics between 3 and 20 were calculated and plotted, corresponding to the minimum error. The smallest error value is calculated at the sixth harmonic in Figure 12. In Figure 13, the NFG
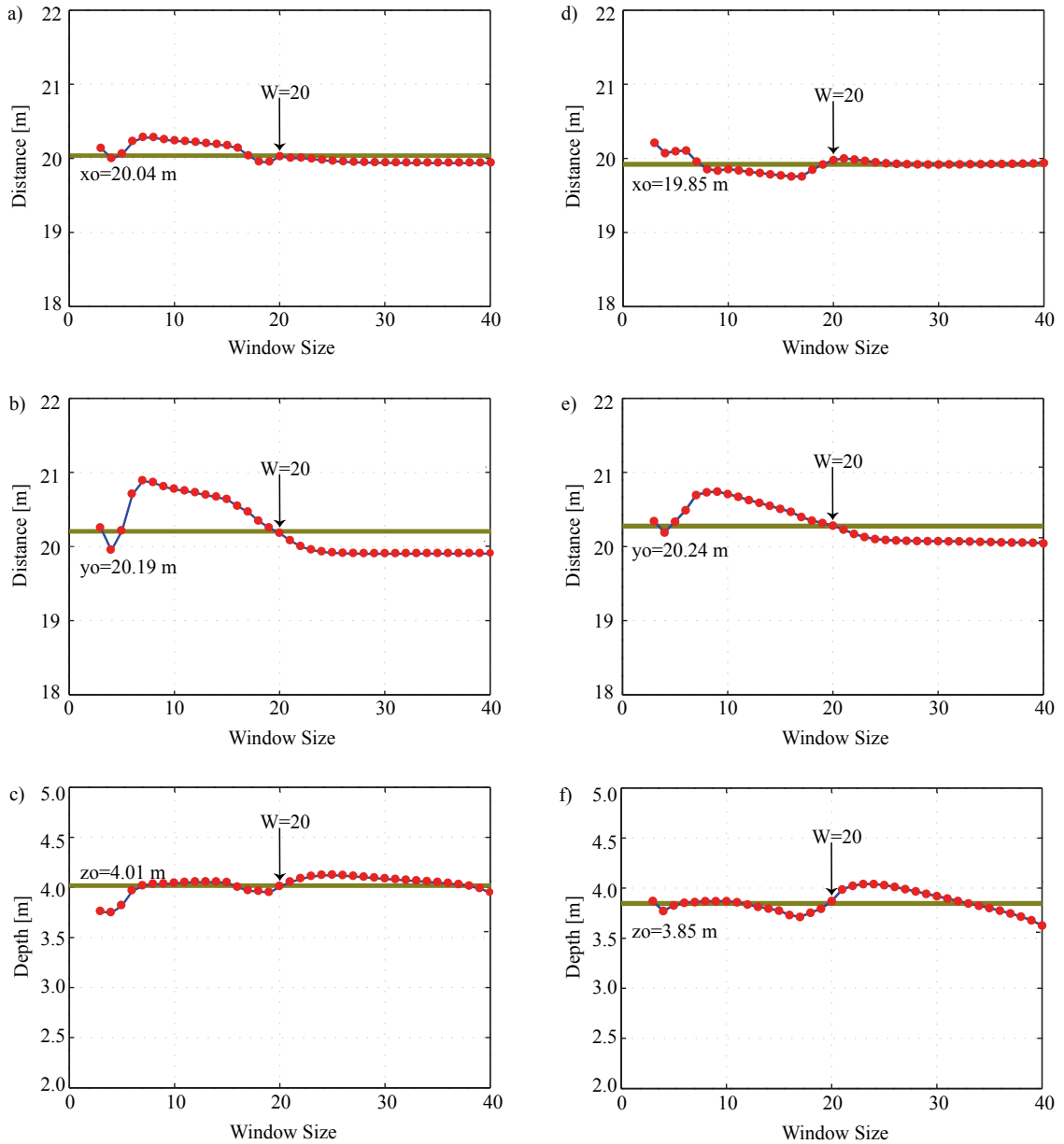
Figure 9. EUD solutions of the synthetic 3D sphere model using mean value calculation. In the case of noise-free data, determination of the window size corresponding to the horizontal distances a) x_0 and b) y_0, and c) the depth (z_0). In the case of noisy data, determination of the window size corresponding to the horizontal distances d) x_0 and e) y_0, and f) the depth (z_0).

cross sections are given for harmonic numbers 5, 6, 7, and 8. The minimum and maximum NFG singular values in the cross sections are marked as white dots. To achieve the correct solution, the minimum and maximum NFG singular values must be at the same depth level. This is achieved in the 6th harmonic. The depth (z_0) and distance (x_0) values obtained from the NFG solution for the 6th harmonic were 39 and 78 m, respectively (Figure 13).

The window sizes were selected between 10 and 60 for the 2D EUD calculation of the Süleymanköy anomaly.

In the EUD method, the parameters can be calculated differently for varied window sizes. Figure 14 shows the calculated location parameters (x_0 and z_0) via the proposed method, for the window sizes in the scale. For example, as seen in Figure 14a, the horizontal distance was calculated as 105 m for window size 10. It was also calculated as 67 m for window size 60. In order to avoid this discrepancy, the average values were calculated. We attempted to determine the optimum window size by calculating the average of the depths (or distances) for each selected window size.
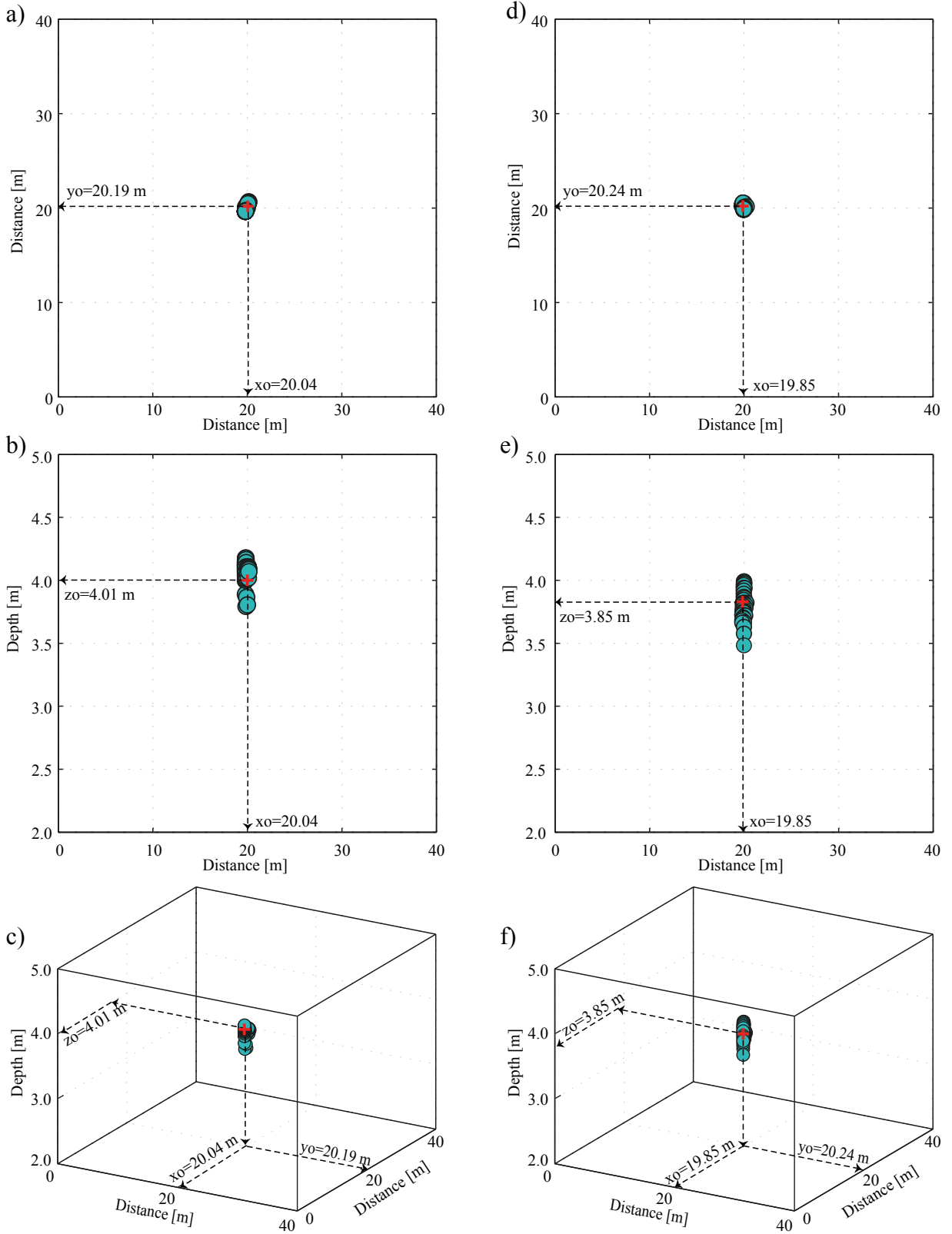
Figure 10. Common solution of depth and horizontal distances from the calculations of the 3D EUD method.

Table 2. The best model parameters obtained from the NFG and EUD algorithms for the synthetic noise-free and noisy datasets (3D).

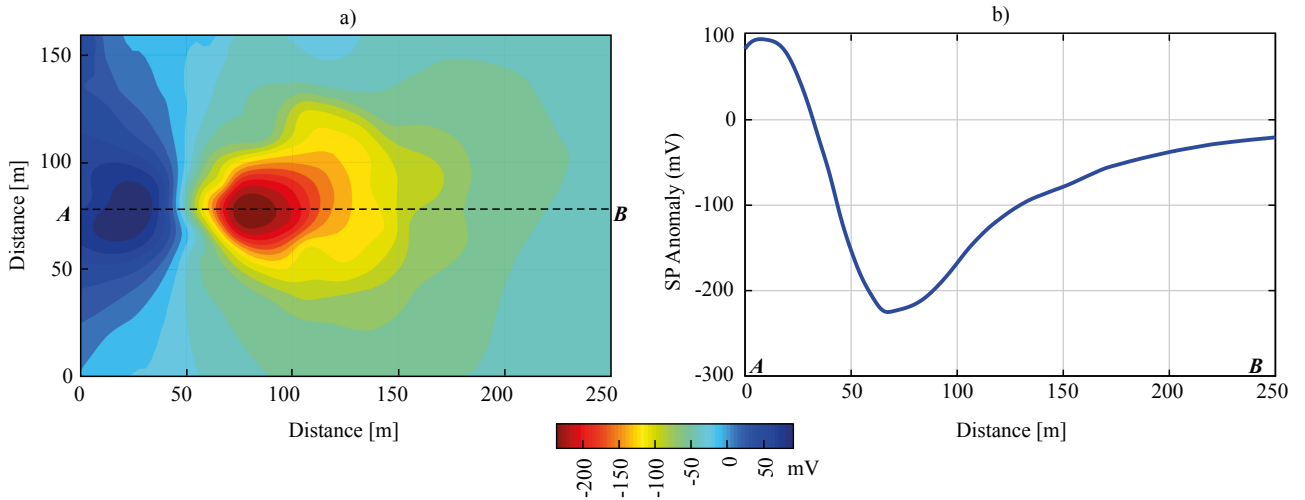| Case	Model par.	Synthetic anomaly	NFG	EUD
Noise-free	z_0 [m]	4.0	4.0	4.01
	x_0 [m]	20.0	20.0	20.04
	y_0 [m]	20.0	20.0	20.19
Noisy	z_0 [m]	4.0	4.5	3.85
	x_0 [m]	20.0	19.0	19.85
	y_0 [m]	20.0	21.0	20.24

Figure 11. a) 3D Süleymanköy SP anomaly, Ergani, Turkey (after Yüngül, 1950), b) AB cross-section over the anomaly digitized with 1-m sampling interval.
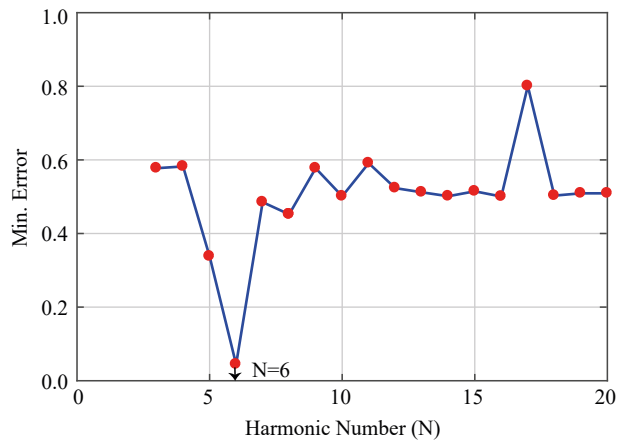

Figure 12. Variations in harmonics corresponding to minimum error values for the Süleymanköy anomaly.
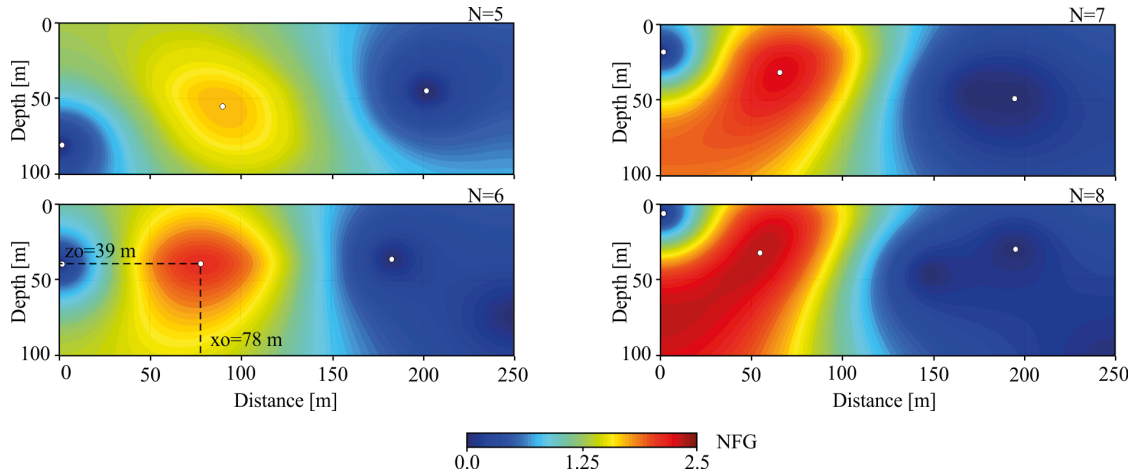
Figure 13. NFG cross-sections for various harmonics and depth (z_0) and distance (x_0) values obtained from the solution for the 6th harmonic for the Süleymanköy anomaly.
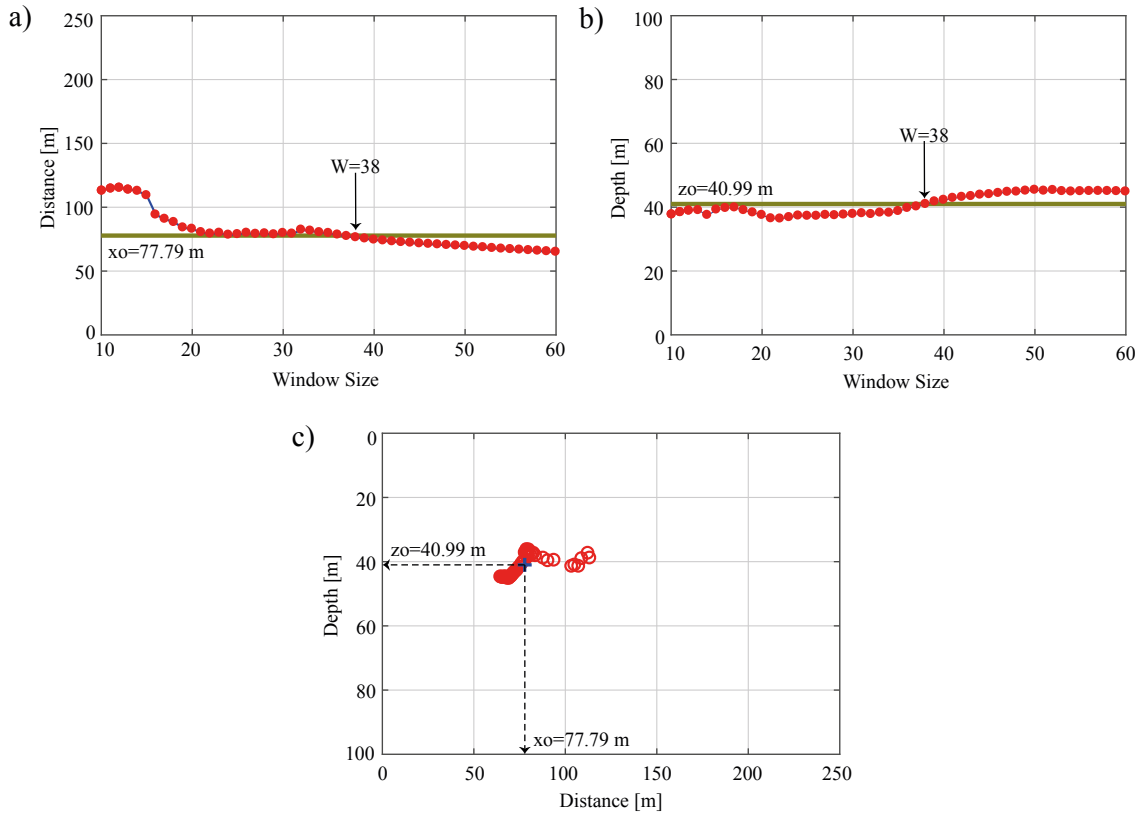

Figure 14. 2D EUD solutions of Süleymanköy anomaly using mean value calculation. Determination of the window size (W = 38) corresponding to the horizontal distance a) x_0 and b) depth (z_0), and c) common solution of depth (z_0) and horizontal distance (x_0).

The horizontal distance from the origin (x_0) and depth of the body (z_0) were calculated as 77.79 m (Figure 14a) and 40.99 m (Figure 14b), respectively. The optimum window size was calculated as 38. The common solution of the horizontal distance from the origin and the depth from the surface is shown in Figure 14c.

The method proposed by Aghajani et al. (2009) in the synthetic model tests was used to determine the number of harmonics in the 3D NFG solutions of the Süleymanköy SP anomaly. Harmonic numbers were selected between 4 and 25. It can be seen from Figure 15a that the maximum NFG amplitude value ($A = 3.18$) was

calculated at the 11th harmonic (Figure 15a). Therefore, $N = 11$ was the optimum harmonic number. Variations in the maximum amplitudes versus depths for the data are plotted in Figure 15b. For each harmonic number, the increase in depth is chosen as 0.5 m. Figure 15b shows the maximum NFG amplitude calculated for $N =$

11 and it was caused by a body with a central depth of about 36.5 m.

When the NFG solutions were plotted at various depth levels for the optimum harmonic number ($N = 11$) (Figure 16), the maximum of the NFG amplitude was reached at 36.5 m in depth and $x_0 = 74$ m and $y_0 = 86$ m in horizontal
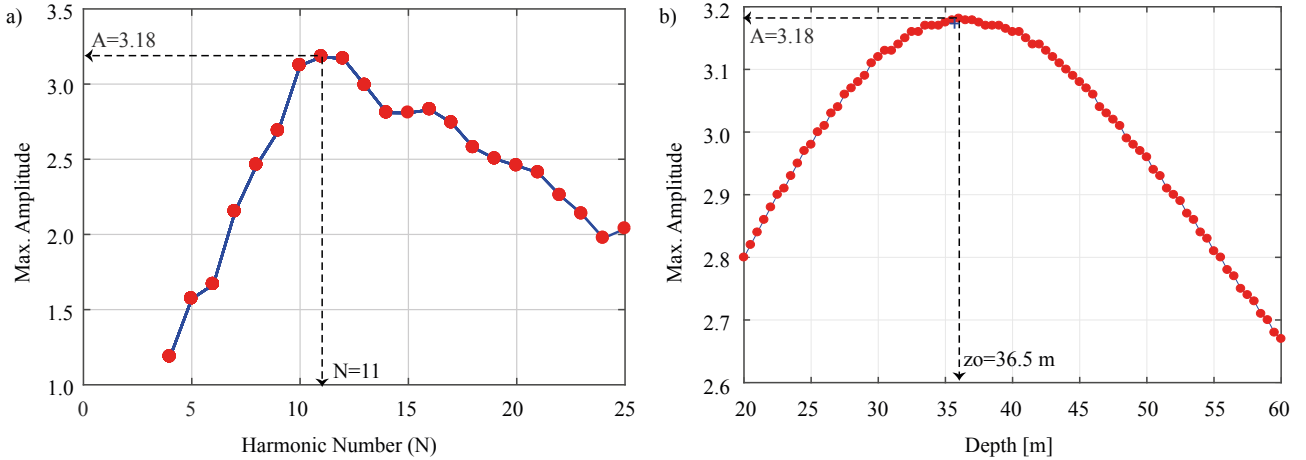

Figure 15. Application of 3D NFG method to the Süleymanköy anomaly: a) calculated maximum amplitudes for different harmonic numbers (N), b) variations in the maximum amplitudes versus depths.
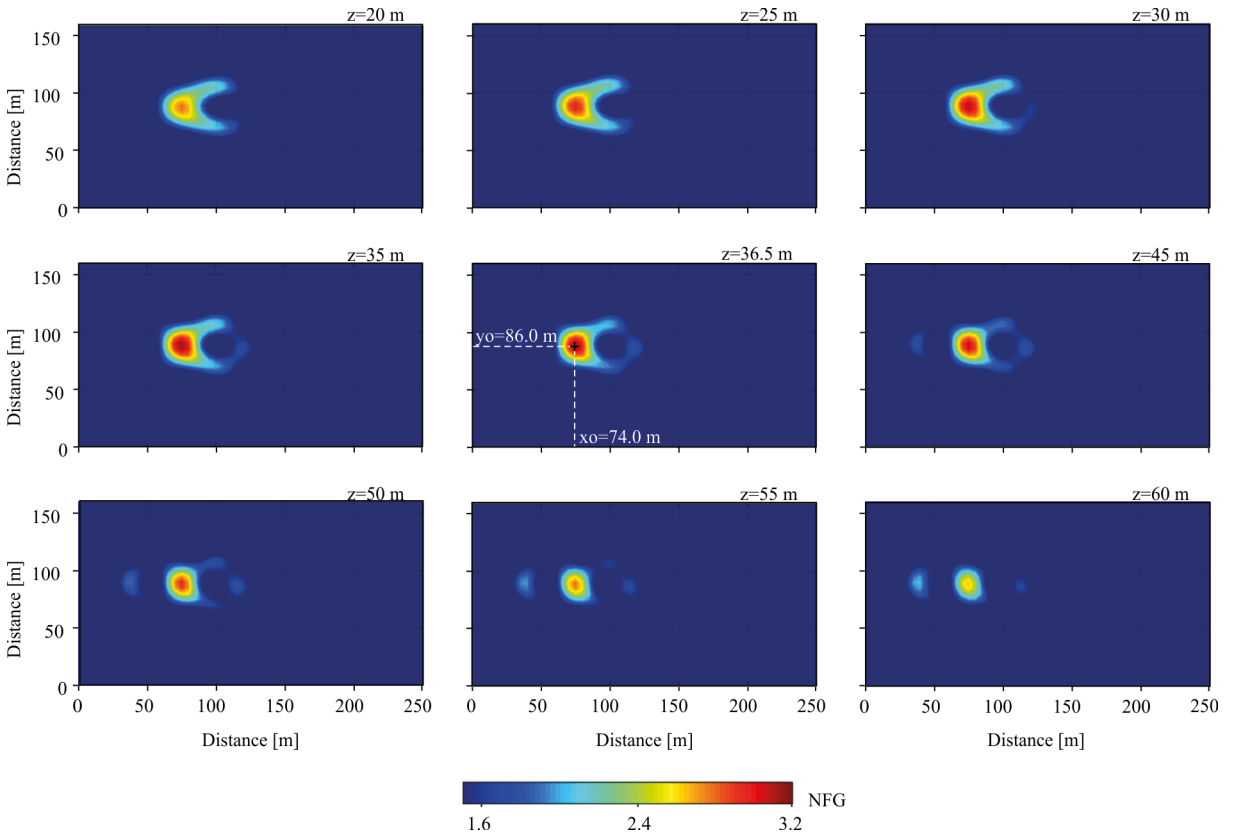

Figure 16. 3D NFG method solutions at various depth levels for the 11th harmonic and calculated location parameters of the Süleymanköy anomaly.

distances, although the NFG contour closures between 30 and 45 m depth were similar.

Finally, the 3D EUD method was applied to analyze the Süleymanköy SP anomaly. The window size was selected between 15 and 40. It can be seen in Figure 17a that the calculated depth is 61 m when the selected window length w = 20 and 80 m when w = 40. Therefore, the average value calculation is applied again. The horizontal distances from the origin (x_0 and y_0) and the depth of the body (z_0)

are calculated as x_0 = 71.25 m (Figure 17a), y_0 = 87.86 m (Figure 17b), and z_0 = 40.11 m (Figure 17c), respectively. The optimum window size was calculated as 29. The common solutions of the horizontal distances from the origin and the depth from the surface are shown in Figures 17d–17f.

Table 3 shows the estimated parameters of the Süleymanköy anomaly via 2D and 3D NFG and EUD methods. Table 4 compares the results of the application of
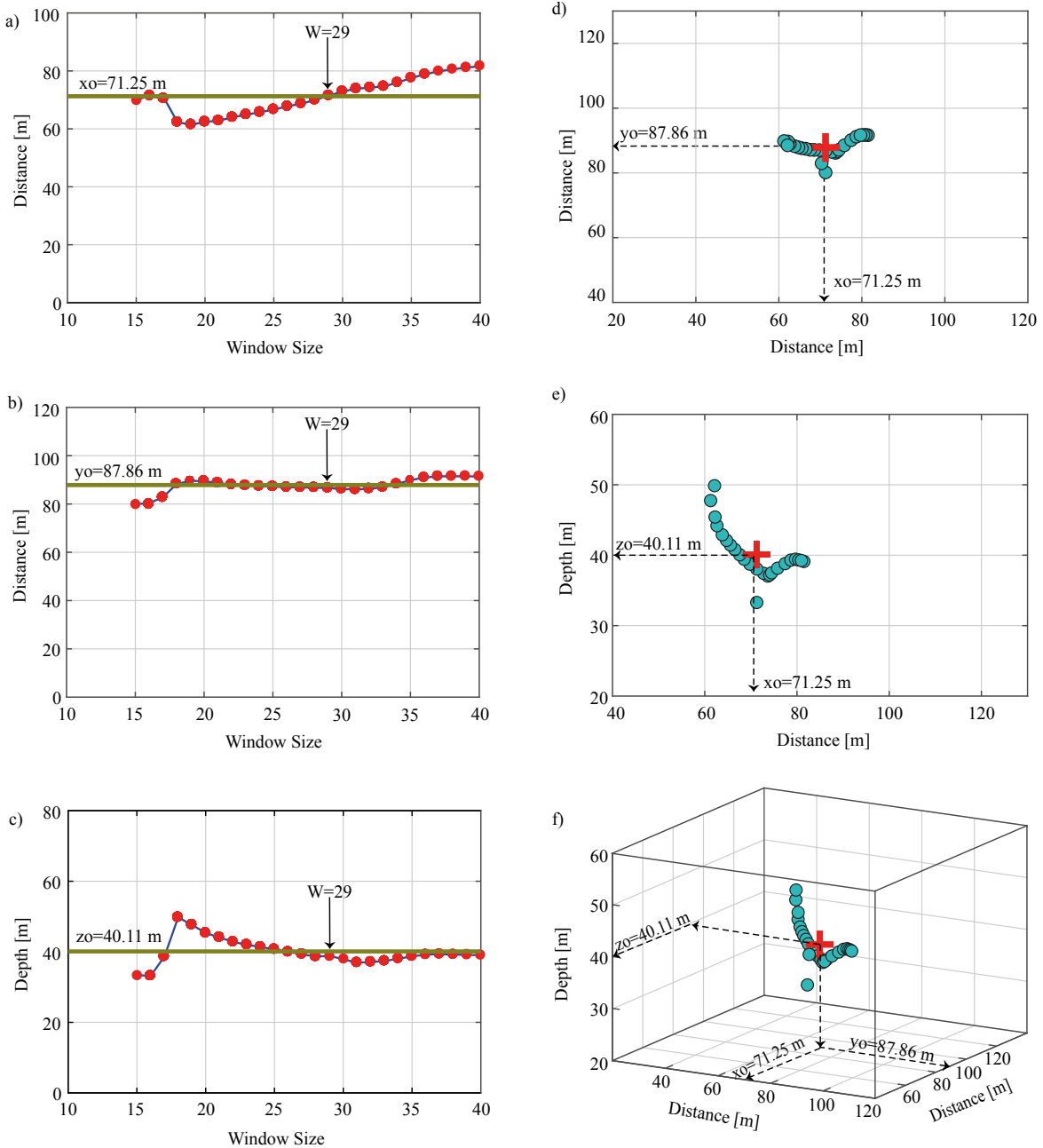

Figure 17. 3D EUD solutions of the Süleymanköy anomaly using average value calculation. Determination of the window size for the horizontal distances a) x_0 and b) y_0, and c) for the depth (z_0). d) Common solution of the horizontal distances x_0 and y_0.

2D and 3D NFG and EUD methods to the Süleymanköy anomaly from this work with those from previous works.

5. Results and discussion

In the present study, 2D and 3D NFG and EUD methods were used to detect the location of a 2D or 3D polarized body having a simple spherical geometry. The methods were tested on both synthetic and field datasets. Although there are many previous studies having 2D and 3D NFG and EUD applications to other potential field such as gravity and magnetic, the present study is the first 3D application of the proposed methods to the SP anomaly caused by the sphere-like model in the literature. In this way, while x- and y-directional NFG and EUD components provide the edge information, z-directional NFG and EUD methods mainly describe the center depth of the body. Although the other optimization techniques provide estimations for more parameters, the 2D and 3D NFG methods can reduce the Gibbs effect and supply reliable information about the location estimation. Therefore, they can be used as complementary approaches to other optimization techniques, especially in studies where it is important to identify the source location in 3D. These results also showed that the proposed methods promise to be useful for determining the boundaries of 3D structures, such as ore deposits. The field data used in the present study are also acquired in an ore site in Turkey. When the calculated location parameters by the proposed methods are compared to the results from the previous studies, they present a good match with each other. Different from the previous studies in this field, the source location parameter in the y-direction was determined with 3D NFG and EUD applications.

Another difference of this study from previous ones was that new criteria for the NFG and EUD methods were developed instead of the trial-and-error method. In 2D NFG method applications, the optimum harmonic number was obtained by calculating the minimum error values corresponding to different harmonic numbers. For the 3D NFG method, this application is not preferred because it must be repeated for each depth level. Instead Agajhani et al.'s (2009) method was used. A new criterion was also developed to determine the optimum window size in the EUD. This criterion was based on the calculation of the average depths (or distances) for each selected window size. According to these criteria, satisfactory results were obtained when applying the NFG and the EUD to noisy as well as noiseless data. When the data were contaminated by noise, we were still able to detect the model parameters with low error levels.

To test the efficiency of the two proposed criteria for the higher noise level (±10 mV), we add noise based on normally distributed, zero-mean pseudorandom numbers

Table 3. The best model parameters obtained from the NFG and EUD algorithms for the Süleymanköy SP anomaly.

Dimension	Model par.	NFG	EUD
2D	z_0 [m]	39.0	40.99
	x_0 [m]	78.0	77.79
3D	z_0 [m]	36.5	40.11
	x_0 [m]	74.0	71.25
	y_0 [m]	86.0	87.86

Table 4. Previous and present studies' (NFG and EUD) results for the Süleymanköy anomaly.

Parameters [m]			Studies
y_0	x_0	z_0	
	78.0	39.0	NFG (2D) (Present study)
	77.8	41.0	EUD (2D) (Present study)
86.0	74.0	36.5	NFG (3D) (Present study)
87.9	71.3	40.1	EUD (3D) (Present study)
	76.7	38.9	Yüngül (1950)
	70,0	40.0	Bhattacharya and Roy (1981)
	66.4	41.4	Ram Babu and Rao (1988)
		36.0	Sundararajan and Srinivas (1996)
		42.0	Abdelrahman and Sharafeldin (1997)
		38.8	Abdelrahman et al. (1997)
		47.6	El-Araby (2004)
		46.8	Abdelrahman et al. (2006)
		35.4	Tlas and Asfahani (2008)
		35.9	Essa et al. (2008)
		38.0	Sındırgı et al. (2008)
		28.9	Srivastava and Agarwal (2009)
	62.3	32.5	Pekşen et al. (2011)
		33.6	Göktürkler and Balkaya (2012)

to the same synthetic SP data, but the resulting plots are not presented here. The depths were calculated for NFG and EUD as 2.5 and 2.6 m, respectively. Moreover, x_0 was calculated for NFG and EUD as 20.3 and 19.14 m, respectively. These results showed that the noise rate higher than ±10 mV (12%) made the estimation of the location parameters difficult, especially depth.

The aim of this study was to estimate the location of the structure for a single sphere model in the SP method with the 2D and 3D NFG and EUD methods. It can be said that both methods provide successful and effective results with the help of the newly introduced criteria.

References

Abdelazeem M, Gobashy M (2006). Self-potential inversion using genetic algorithm. Journal of King Abdulaziz University - Earth Sciences 17: 83-101.

Abdelrahman EM, Ammar AA, Hassanein HI, Hafez MA (1998). Derivative analysis of SP anomalies. Geophysics 63: 890-897.

Abdelrahman EM, Ammar AA, Sharafeldin SM, Hassanein HI (1997). Shape and depth solutions from numerical horizontal self-potential gradients. Applied Geophysics 36: 31-43.

Abdelrahman EM, El-Araby HM, Hassaneen AG, Hafez MA (2003). New methods for shape and depth determination from SP data. Geophysics 68: 1202-1210.

Abdelrahman EM, Sharafeldin SM (1997). A least-squares approach to depth determination from residual self-potential anomalies caused by horizontal cylinders and spheres. Geophysics 62: 44-48.

Abedi M, Hafizi MK, Norouzi GH (2012). 2D interpretation of self-potential data using Normalized Full Gradient, a case study: galena deposit. Bollettino di Geofisica Teorica ed Applicata 53: 213-230.

Agarwal BNP, Srivastava S (2009). Analyses of self-potential anomalies by conventional and extended Euler deconvolution techniques. Computers & Geosciences 35: 2231-2238.

Aghajani H, Moradzadeh A, Zeng H (2009). Normalized full gradient of gravity anomaly method and its application to the Mobrun Sulfide Body, Canada. World Applied Sciences Journal 6: 392-400.

Aghajani H, Moradzadeh A, Zeng H (2011). Detection of high-potential oil and gas fields using normalized full gradient of gravity anomalies: a case study in the Tabas Basin, Eastern Iran. Pure and Applied Geophysics 168: 1851-1863.

Al-Saud MM (2014). The role of aeromagnetic data analysis (using 3D Euler deconvolution) in delineating active subsurface structures in the west central Arabian shield and the central Red Sea, Saudi Arabia. Arabian Journal of Geosciences 7: 4361-4376.

Asfahani J, Tlas M, Hammadi M (2001). Fourier analysis for quantitative interpretation of self-potential anomalies caused by horizontal cylinder and sphere. Journal of King Abdulaziz University - Earth Sciences 13: 41-53.

Aydın A (2007). Interpretation of gravity anomalies with the normalized full gradient (NFG) method and an example. Pure and Applied Geophysics 164: 2329-2344.

Aydın A (2010). Application of the normalized full gradient (NFG) method to resistivity data. Turkish Journal of Earth Sciences 19: 513-526.

Balkaya Ç (2013). An implementation of differential evolution algorithm for inversion of geoelectrical data. Journal of Applied Geophysics 98: 160-175.

Beasley CW, Golden HC (1993). Application of Euler Deconvolution to magnetic data from the Ashanti belt, southern Ghana. In: 63rd Annual International Meeting, Society of Exploration Geophysicists, pp. 417-420.

Berezkin VM (1967). Application of the total vertical gradient of gravity for determination of the depths to the sources of gravity anomalies. Exploration Geophysics 18: 69-79.

Berezkin VM (1973). Application of Gravity Exploration to Reconnaissance of Oil and Gas Reservoir. Moscow, USSR: Nedra Publishing House.

Berezkin VM (1988). Full Gradient Method in Geophysical Prospecting. Moscow, USSR: Nedra Publishing House.

Bhattacharya BB, Roy N (1981). A note on the use of a nomogram for self-potential anomalies. Geophysical Prospecting 29: 102-104.

Biswas A, Sharma SP (2015). Interpretation of self-potential anomaly over idealized body and analysis of ambiguity using very fast simulated annealing global optimization. Near Surface Geophysics 13: 179-195.

Bogoslovsky VA, Ogivly AA (1973). Deformations of natural electric fields near drainage structures. Geophysical Prospecting 21: 716-723.

Ciancara B, Marcak H (1979). Geophysical anomaly interpretation of potential fields by means of singular points method and filtering. Geophysical Prospecting 27: 251-260.

Corwin RF (1990). The self-potential method for environmental and engineering applications. In: Ward H (editor). Geotechnical and Environmental Geophysics. Tulsa, OK, USA: Society of Exploration Geophysicists, pp. 127-145.

Dewangan P, Ramprasad T, Ramana MV, Desa M, Shailaja B (2007). Automatic interpretation of magnetic data using Euler deconvolution with nonlinear background. Pure and Applied Geophysics 164: 2359-2372.

Di Maio R, Piegari E, Rani P, Avella A (2016). Self-potential data inversion through the integration of spectral analysis and tomographic approaches. Geophysical Journal International 206: 1204-1220.

Di Maio R, Rani P, Piegari E, Milano L (2017a). Self-potential data inversion through a Genetic-Price Algorithm. Computers & Geosciences 94: 86-95.

Di Maio, R Rani P, Piegari E, Rani P (2017b). Source depth estimation of self-potential anomalies by spectral methods. Journal of Applied Geophysics 136: 315-325.

Dondurur D (2005). Depth estimates for Slingram electromagnetic anomalies from dipping sheet-like bodies by the normalized full gradient method. Pure and Applied Geophysics 161: 2179-2196.

Ebrahimzadeh Ardestani V (2004). Detection of near-surface anomalies through 2-D normalized full gradient of gravity data. Journal of the Earth and Space Physics 30: 1-6.

Ekinci YL, Balkaya Ç, Şeren A, Kaya MA, Lightfoot CS (2014). Geomagnetic and geoelectrical prospection for buried archaeological remains on the upper city of Amorium, a Byzantine city in midwestern Anatolia Turkey. Journal of Geophysics and Engineering 11: 015012.

Ekinci YL, Özyalın Ş, Sındırgı P, Balkaya Ç, Göktürkler G (2017). Amplitude inversion of 2D analytic signal of magnetic anomalies through differential evolution algorithm. Journal of Geophysics and Engineering 14(6): 1492-1508.

Ekinci YL, Yiğitbaş E (2012). A geophysical approach to the igneous rocks in the Biga Peninsula (NW Turkey) based on airborne magnetic anomalies: geological implications. Geodinamica Acta 25: 267-285.

Ekinci YL, Yiğitbaş E (2015). Interpretation of gravity anomalies to delineate some structural features of Biga and Gelibolu peninsulas and their surroundings (north-west Turkey). Geodinamica Acta 27: 300-319.

El-Araby H (2004). A new method for complete quantitative interpretation of self-potential anomalies. Journal of Applied Geophysics 55: 211-224.

Essa K, Elhussein M (2017). A new approach for the interpretation of self-potential data by 2-D inclined plate. Journal of Applied Geophysics 136: 455-461.

Essa K, Mehanee S, Smith PD (2008). A new inversion algorithm for estimating the best fitting parameters of some geometrically simple body to measured self-potential anomalies. Exploration Geophysics 39: 155-163.

Fairhead JD, Misener JD, Green CM, Bainbridge G, Reford SW (1997). Large scale compilations of magnetic, gravity, radiometric and electromagnetic data: the new exploration strategy for the 90s. In: Proceedings of Exploration 97: Fourth Decennial International Conference on Mineral Exploration, pp. 805-816.

Fedi M, Abbas M (2013). A fast interpretation of self-potential data using the depth from extreme points method. Geophysics 78: E107-E116.

Fedi M, Florio G (2011). Normalized downward continuation of potential fields within the quasi-harmonic region. Geophysical Prospecting 59: 1087-1100.

Fernández-Martínez JL, García-Gonzalo E, Naudet V (2010). Particle swarm optimization applied to solving and appraising the streaming-potential inverse problem. Geophysics 75: WA3-WA15.

Fitzgerald DJ, Reid AB, McInerney P (2004). New discrimination techniques for Euler deconvolution. Computers and Geosciences 30: 461-469.

Gerovska D, Arauzo-Bravo M (2003). Automatic interpretation of magnetic data based on Euler deconvolution with unprescribed structural index. Computers and Geosciences 29: 949-960.

Göktürkler G, Balkaya Ç (2012). Inversion of self-potential anomalies caused by simple geometry bodies using global optimization algorithms. Journal of Geophysics and Engineering 9: 498-507.

Golizdra GY (1962). On relationship between singular points of gravity potential and form anomalous masses. In: 2nd Conference of Young Geologists of Ukraine Proceedings, Kyiv.

Hearst RB, Morris WA (1993). Interpretation of the Sudbury structure through Euler deconvolution. In: 63rd Annual International Meeting, Society of Exploration Geophysicists, pp. 421-424.

Hou Z, Shi Z (1986). Implementation of the normalized total gradient of gravitational-magnetic anomaly by Fourier integration. Geophysical Prospecting for Petroleum 25: 75-86.

Jung K (1961). Schwerkraftverfahren in der angewandten Geophysik. Leipzig, Germany: Akademische Verlagsgesellschaft Gees und Portig KG (in German).

Keating P, Pilkington M (2004). Euler deconvolution of the analytic signal and its application to magnetic interpretation. Geophysical Prospecting 53: 165-182.

Meiser P (1962). A method of quantitative interpretation of self-potential measurements. Geophysical Prospecting 10: 203-218.

Mendonça CA (2008). Forward and inverse self-potential modeling in mineral exploration. Geophysics 73: F33-F43.

Mohan V, Singh R (1972). Quantitative interpretation of self-potential anomalies due to spherical ore bodies. Pure and Applied Geophysics 80: 134-139.

Mudretsova EA, Varlamov AS, Filatov VG, Komarova GM (1979). The interpretation of detailed gravity data over the nonstructural oil and gas reservoirs. Moscow, USSR: Nedra Publishing House.

Murthy BVS, Haricharan P (1984). SP anomaly over double line of poles, interpretation through log curves. Proceedings of the Indian Academy of Sciences - Earth & Planetary Sciences 93: 437-445.

Murthy BVS, Haricharan P (1985). Nomograms for the complete interpretation of spontaneous potential profiles over sheet-like and cylindrical two-dimensional sources. Geophysics 50: 1127-1135.

Mushayandebvu MF, van Driel P, Reid AB, Fairhead JD (2001). Magnetic source parameters of two-dimensional structures using extended Euler deconvolution. Geophysics 66: 814-823.

Oruç B, Keskinsezer A (2008). Detection of causative bodies by normalized full gradient of aeromagnetic anomalies from east Marmara region, NW Turkey. Journal of Applied Geophysics 65: 39-49.

Özyalın Ş (2003). Automated interpretation methods in potential fields and application to the archeological sites. PhD, Dokuz Eylül University, İzmir, Turkey.

Pašteka R (1996). Properties of the total normalised gradient of potential function for the determination of source distributions. In: Proceedings of the 7th International Meeting on Alpine Gravimetry, Vienna, pp. 187-207.

Pašteka R (2000). 2D semi-automated and environmental methods in gravimetry and magnetometry. Acta Geologica Universitatis Comenianae 55: 5-50.

Paterson NR, Kwan KCH, Reford SW (1991). Use of Euler deconvolution in recognizing magnetic anomalies of pipe-like bodies. In: 61st Annual International Meeting, Society of Exploration Geophysicists, pp. 642-645.

Paul MK (1965). Direct interpretation of self-potential anomalies caused by inclined sheets of infinite horizontal extensions. Geophysics 30: 418-423.

Paul MK, Datta S, Banerjee B (1965). Interpretation of self potential anomalies due to localized causative bodies. Pure and Applied Geophysics 61: 95-100.

Pekşen E, Yas T, Kayman AY, Özkan C (2011). Application of particle swarm optimization on self-potential data. Journal of Applied Geophysics 75: 305-318.

Rabeh T, Khalil A (2015). Characterization of fault structures in southern Sinai Peninsula and Gulf of Suez region using geophysical data. Environmental Earth Sciences 73: 1925-1937.

Rao AD, Ram Babu HV (1983). Quantitative interpretation of self-potential anomalies due to two-dimensional sheet like bodies. Geophysics 48: 1659-664.

Rao BSR, Murthy IVR, Reddy SJ (1970). Interpretation of self-potential anomalies of some simple geometrical bodies. Pure and Applied Geophysics 78: 60-77.

Reid AB, Allsop JM, Granser H, Milett AJ, Somerton I (1990). Magnetic interpretation in three dimensions using Euler deconvolution. Geophysics 55: 80-91.

Revil A, Jardani A (2013). The Self-Potential Method: Theory and Applications in Environmental Geosciences. New York, NY, USA: Cambridge University Press.

Rikitake T, Sato R, Hagiwara Y (1976). Applied Mathematics for Earth Scientists. Tokyo, Japan: Terra Scientific.

Roest WR, Verhoef J, Pikington M (1992). Magnetic interpretation using the 3-D analytic signal. Geophysics 57: 116-125.

Roy SVS, Mohan NL (1984). Spectral interpretation of self potential anomalies of some simple geometric bodies. Pure and Applied Geophysics 78: 66-77.

Santos FAM (2010). Inversion of self-potential of idealized bodies anomalies using particle swarm optimization. Computers & Geosciences 36: 1185-1190.

Schima S, Wilt M, Ross H (1996). Modeling Self-Potential Data in the Abraham and Meadow-Hatton Geothermal Systems. Washington, DC, USA: US Department of Energy Research Summaries.

Sill WR (1983). Self-potential modelling from primary flows. Geophysics 48: 76-86.

Silva JBC, Barbosa VCF (2003). 3D Euler Deconvolution: theoretical basis for automatically selecting good solutions Geophysics 68: 1962-1968.

Silva JBC, Barbosa VCF, Medeiros WE (2001). Scattering, symmetry, and bias analysis of source position estimates in Euler deconvolution and its practical implications. Geophysics 66: 1149-1156.

Sındırgı P, Pamukçu O, Özyalın Ş (2008). Application of normalized full gradient method to self potential (SP) data. Pure and Applied Geophysics 165: 409-427.

Srivastava S, Agarwal BNP (2009). Interpretation of self-potential anomalies by enhanced local wave number technique. Journal of Applied Geophysics 68: 259-268.

Strakhov VN (1962). On the ways to constructing mathematical theory of interpretation of magnetic and gravity anomalies, Prikladnaya Geofizika 36: 95-128.

Strakhov VN, Grigoreva OM, Lapina MI (1977). Determination of singular points of two dimensional potential fields. Prikladnaya Geofizika 85: 96-113.

Sundararajan N, Arun Kumar I, Mohan NL Seshagiri Rao SV (1990). Use of the Hilbert transform to interpret self-potential anomalies due to two-dimensional inclined sheets. Pure and Applied Geophysics 133: 117-126.

Sundararajan N, Narasimha Chary M (1993). Direct interpretation of self-potential anomalies due to spherical structures - a Hilbert transform technique. Geophysical Transactions 38: 151-165.

Sundararajan N, Sirinivas Y (1996). A modified Hilbert Transform and its application to self potential interpretation. Journal of Applied Geophysics 36: 137-143.

Thompson DT (1982). EULDPH: A technique for making computer assisted depth estimates from magnetic data. Geophysics 47: 31-37.

Tlas M, Asfahani J (2008). Using of the adaptive simulated annealing (ASA) for quantitative interpretation of self-potential anomalies due to simple geometrical structures. Journal of King Abdulaziz University 19: 99-118.

Tran TD (2004). Two and three dimensional normalized total gradient of gravity anomalies and its application for detecting the oil-gas potential areas in the southeast sedimentary basins of the East Vietnam Sea. In: Proceedings of the 7th SEGJ International Symposium-Imaging Technology, Sendai, Japan, p. 6.

Yasukawa K, Mogi T, Widarto D, Ehara S (2003). Numerical modeling of a hydrothermal system around Waita Volcano, Kyushu, Japan, based on resistivity and self-potential survey results. Geothermics 32: 21-46.

Yüngül S (1950). Interpretation of spontaneous polarization anomalies caused by spherical ore bodies. Geophysics 15: 237-246.

Zeng H, Meng X, Yao C, Li X, Lou H et al. (2002). Detection of reservoirs from normalized full gradient of gravity anomalies and its application to Shengli oil field, east China. Geophysics 67: 1138-1147.

Zhang CY, Mushayandebvu MF, Reid AB, Fairhead JD, Odegard ME (2000). Euler deconvolution of gravity tensor gradient data. Geophysics 65: 512-520.

Zhang S, Meng X (2015). Improved normalized full-gradient method and its application to the location of source body. Journal of Applied Geophysics 113: 86-91.

Zhou W (2015). Normalized full gradient of full tensor gravity gradient based on adaptive iterative Tikhonov regularization downward continuation. Journal of Applied Geophysics 118: 75-83.